Vacancy Ordering in *O*3-Type Layered Metal Oxide Sodium-Ion Battery Cathodes

Alexandra J. Toumar,[1] Shyue Ping Ong,[2] William Davidson Richards,[1] Stephen Dacek,[1] and Gerbrand Ceder[1,*]

[1]*Department of Materials Science and Engineering, Massachusetts Institute of Technology, Cambridge, Massachusetts 02139, USA*

[2]*Department of NanoEngineering, University of California, San Diego, La Jolla, California 92093, USA*

(Received 15 May 2015; revised manuscript received 9 November 2015; published 11 December 2015)

Current state-of-the-art Na-ion battery cathodes are selected from the broad chemical space of layered first-row transition-metal (TM) oxides. Unlike their lithium-ion counterparts, seven first-row layered TM oxides can intercalate Na ions reversibly. Their voltage curves indicate significant and numerous reversible phase transformations during electrochemical cycling. These transformations are not yet fully understood but arise from Na-ion vacancy ordering and metal oxide slab glide. In this study, we investigate the nature of vacancy ordering within the *O*3 host lattice framework. We generate predicted electrochemical voltage curves for each of the Na-ion intercalating layered TM oxides by using a high-throughput framework of density-functional-theory calculations. We determine a set of vacancy-ordered phases appearing as ground states in all Na_xMO_2 systems and investigate the energy effect of the stacking of adjacent layers.

DOI: 10.1103/PhysRevApplied.4.064002

I. INTRODUCTION

Sodium-ion batteries have been highlighted in recent years for their potential as an inexpensive, geopolitically neutral alternative to Li-based rechargeable batteries, largely due to the global abundance and low cost of sodium-containing precursor materials [1]. The number of layered transition-metal oxide compounds that can intercalate Na ions reversibly is large compared to its Li-ion counterparts, implying a much broader chemical space in which electrode materials can be optimized. This, together with sodium's abundance, balances the disadvantage in energy density due to the standard potential of Na^+, making Na-ion batteries excellent candidates for large-scale energy storage [2,3]. Theoretical work [4] points out the fundamental difference between Na and Li intercalation that makes Na cathodes more stable against transformation into other structures. Vast progress has been made in the exploration of potential cathode, anode, and electrolyte materials for Na-ion batteries, with publications relating to sodium energy-storage materials increasing to over 120 per year in 2013 [5].

Na-ion intercalating transition-metal oxides were first studied for their potential electrochemical properties in the 1980s, showing reversible Na intercalation for seven layered oxide systems with 3d transition metals (TMs): Na_xMO_2 (M = Ti [6], V [7], Cr [8,9], Mn [10], Fe [11], Co [12], and Ni [8]). This is in sharp contrast to their Li equivalents, which reversibly exchange Li only for M = Co and Ni [4,9,13]. Several layered Na-TM oxides approach the energy densities of their Li-ion counterparts. In particular, mixed TM oxides can deliver specific energy densities close to 600 Wh/kg [for example, $Na(Mn_{0.25}Fe_{0.25}Co_{0.25}Ni_{0.25})O_2$ delivers 578 Wh/kg] [14], with single TM oxides such as Na_xMnO_2 reaching capacities of nearly 200 mA h/g [15].

Reversible intercalation of Na ions from layered TM oxide hosts results in several reversible first-order phase transformations appearing as large steps and plateaus in the electrochemical voltage curve. Such steps are most numerous and apparent in single TM oxide systems, such as *O*3-type $NaNiO_2$ [16], *O*3-type $NaMnO_2$ [15], *O*3-$NaVO_2$ [17], and *P*2-$NaVO_2$ [18] (here *O*3 and *P*2 refer to the Delmas naming convention [19]). These phase transitions have been found to result from sodium vacancy ordering and the gliding of TM oxide layers and are apparent even at the highest cycling rates cited in the literature (typically $C/10$) [15,16]. While Li-intercalating layered TM oxides are synthesizable only in the *O*3 structure, Na-ion intercalating layered oxides demonstrate two types of stacking varieties: *O*3, which can transform reversibly through slab glide to *P*3 [12], and *P*2, which can transform reversibly to *O*2 [20]. Of particular importance is the study of Na-vacancy ordering common between TM chemistries and its driving force. Such Na-vacancy ordering occurs through clear first-order transitions in single TM compounds and therefore can be best studied in these systems. Though some work has been done on predicting alkali ion ordering in several Li-ion and Na-ion systems [21–25], this has been undertaken for the entire intercalation range in only a very few cases and with little comparison between similar systems.

Phase transformations and the shape of the voltage curve can strongly influence the function of a battery cathode material. A voltage curve with many large

*To whom all correspondence should be addressed.
gceder@mit.edu

first-order phase-transition steps can lead to poor kinetics, because these phase transitions act as an additional energy barrier in moving the Na ions from their octahedral sites. For example, slow kinetics have been evidenced in $O3$-type $NaVO_2$ [7], which shows numerous first-order phase transitions in the experimental voltage curve. Conversely, a recent study in a $P2$-type material shows that, when ordering phase transitions are suppressed, the kinetics and cycle life are excellent [26]. It is thus important to understand these phase transformations to facilitate better material design. The objectives of this study are to explore the low-energy vacancy-ordering transitions within the $O3$-type lattice structure and to draw comparisons across the spectrum of different TM systems. We discover, through an extensive computational search of $O3$-type Na-ion intercalating systems, the vacancy-ordering patterns common to all seven TM systems. We further investigate the magnitude of the ordering energies and the effect of layer stacking, examining the effect of interaction between adjacent Na layers on the total energy.

II. METHODS

This study is restricted to the $O3$-type layered structure as classified by Delmas [19] and its monoclinic derivatives formed by the coordinated distortion of the TM oxide octahedra due to Jahn-Teller instabilities [27] and oxidation state ordering [17]. The $O3$ structure is shown in Fig. 1. We investigate the case of topotactic electrochemical deintercalation, where the fundamental $O3$ structure is not disturbed and there is no ion migration between the TM and Na layers, though the lattice parameters and unit-cell internal degrees of freedom are fully relaxed. The majority of the calculations are performed on unit cells with a single Na-ion layer repeat period perpendicular to the layers. Except for an established structure at 5/8 Na concentration, which has been characterized experimentally and confirmed computationally in previous work [Fig. 6(j)] [27], Na ions are assumed to remain in octahedral sites and not move into highly distorted or tetrahedral sites in the Na layer. All initial structures are obtained by replacing the alkali and Co^{3+} ion in the $R\bar{3}m$ $LiCoO_2$ structure, except in the cases of Jahn-Teller active Ni^{3+} and Mn^{3+} ions where the monoclinic distortion is imposed.

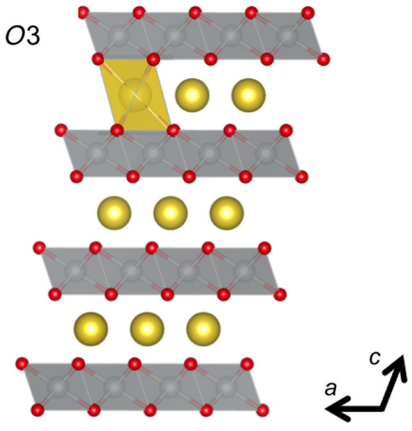

FIG. 1. $O3$-type layered metal oxide structure. Na sits in octahedral sites between layers of metal oxide octahedra; oxygen stacking repeats after three layers.

The energy is calculated for a large trial set of possible Na-vacancy-ordered structures within the layered metal oxide framework. The trial set consists of structures that commonly occur as ground-state orderings on the triangular lattice, such as those determined by Kaburagi and Kanamori [28] to be ground states with up to third-neighbor interactions, as well as the possible ground states for $O3$-$NaCoO_2$ found by Wang, Ding, and Ni [22]. In addition, potential structures are generated at Na concentrations of 1/4, 1/3, 1/2, 2/3, and 3/4. At these concentrations, ground states are predicted for Li intercalating layered oxides, such as Li_xNiO_2 [29]. Potential vacancy orderings at these compositions are generated on supercells restricted to a single Na layer and include repeating patterns up to 12 Na_xMO_2 unit cells in size. Potential structures are generated by using an enumeration algorithm as part of the PYMATGEN [30] code base. For the selected concentrations, between 10 and 60 unique structures are calculated depending on the supercell size, giving a total of approximately 500 calculations for each TM system. The total trial set is then calculated in a high-throughput framework using density-functional theory (DFT) to generate convex energy hulls for each of the seven Na_xMO_2 systems, such as that for the $M = \mathrm{Cr}$ system shown in Fig. 3. From these, any ordering occurring as a ground state in any of the systems is collected, leading to a set of 18 low-energy ordering types.

DFT energy calculations are performed by using the Vienna *Ab Initio* Simulation Package (VASP) [31] within the projector-augmented wave approach [32], using the Perdew-Burke-Ernzerhof generalized-gradient approximation (GGA) [33] functional with the GGA + U extension [34]. Magnetic moments of Co^{3+}, Co^{4+}, Ni^{3+}, and Ni^{4+} ions are initialized as low spin, which is found to improve energy convergence. U corrections for the transition metals are tabulated in Table I and are optimized for transition metals in an oxide environment in a previous work [30].

TABLE I. U values for seven first-row transition metals in an oxide environment.

Element (oxide environment)	U value (eV)
Ti	0.0
V	3.1
Cr	3.5
Mn	3.9
Fe	4.0
Co	3.4
Ni	6.0

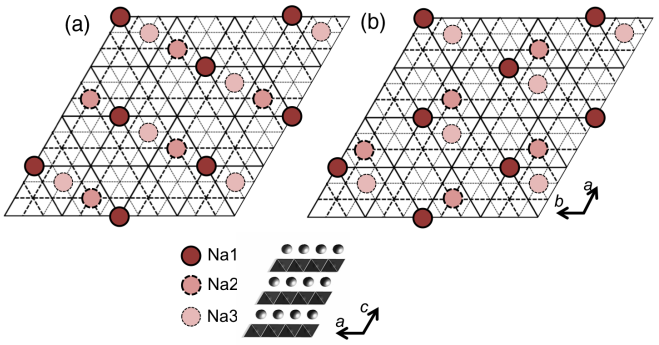

FIG. 2. Different stacking variants of a $Na_{1/3}MO_2$-ordered layer. Three layers are shown by solid, dashed, and dotted lines. Different shades on atoms indicate Na in different layers. (a) and (b) show the two different types of stacking possible if one Na layer is translated in-plane relative to its adjacent layer.

A U correction is not assigned for calculations in the Ti system, to better represent the delocalized nature of electrons in reduced Ti oxides [30]. The average intercalation potential of the cathode is obtained by using energies computed within DFT [4,35]:

$$V = -\frac{E(A_nH) - E(A_{n-x}H) - xE(A)}{xe}, \qquad (1)$$

where A is the alkali ion, H is the host structure, and e is the electronic charge. For each of the 18 orderings appearing as ground states in any of the seven TM systems, we further investigate the effect of interplanar interactions by generating all possible adjacent-layer stacking variants of the ordering along the c axis. These supercells are generated by laterally translating the Na-vacancy-ordering pattern in adjacent layers by all linear combinations of the primitive in-plane lattice vectors for the AMO_2 unit. Symmetrically equivalent stackings are removed from the data set. An example of this is given in Fig. 2, which shows two structures with a projection of three identically ordered Na layers and how these can be positioned relative to one another.

III. RESULTS

A. Single transition-metal ground states

For a Na_xMO_2 system, the convex hull is given by the linear combination of ground states which gives the lowest energy at any composition. A voltage curve is generated from the energy differences of these ground states along the convex hull.

Figures 3 and 4 show the hull and voltage curve for the $O3$-Cr system as an example. Red points on the hull plot indicate computed structures which are higher in energy than the ground-state phases. Blue points on the hull indicate the ordered ground-state structures for the Cr system. The voltage curve in Fig. 4 shows steps corresponding to eight stable phases occurring at 3/4, 2/3, 5/8, 1/2, 2/5, 1/3, 1/4, and 1/7 Na concentrations. As the voltage curve is the result of 0-K calculations, finite-temperature entropy effects are expected to smoothen the curves. The figures surrounding the voltage plot depict the Na-vacancy ordering for each ground state in a single Na layer.

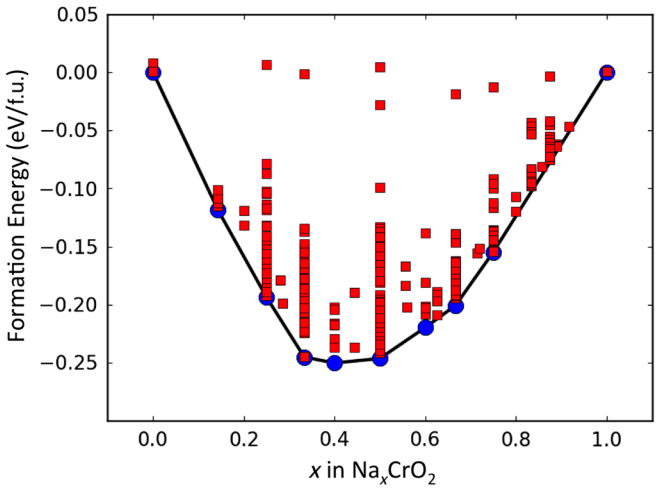

FIG. 3. Calculated energies for Na-vacancy orderings in the Na_xCrO_2 system. Red points indicate the energies of different enumerated single-Na-layer phases computed at that Na concentration. Blue points are ground states, as they are part of the convex energy hull (solid line).

Figure 5 shows the calculated $O3$ voltage curves for all seven Na-intercalating TM oxides. From the computed voltage curves, we see that in all seven $O3$ systems strong phase transitions are predicted to occur at 1/2 and 1/3 Na concentrations, as shown by the large 0.25–0.75-V voltage differences at these steps. The Cr and Mn voltage curves are shallow compared to the other systems, spanning less than 1.5 V (compared to systems such as Ti and V, which span between 1.5 and 3 V). It should be noted that our results indicate that topotactic deintercalation to low Na concentrations leads to high-energy states and, therefore, very high voltages for some systems (e.g., V). It is expected that in

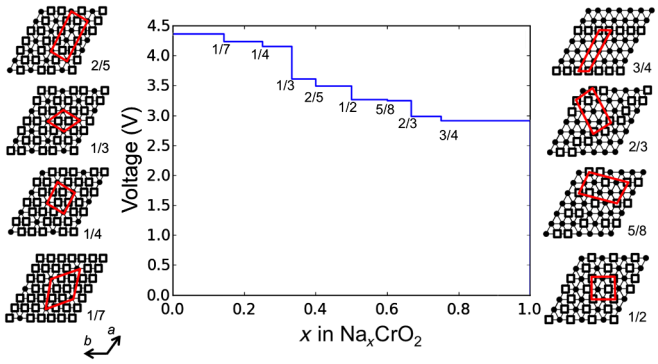

FIG. 4. Computed $O3$-lattice voltage curve with predicted ground-state Na-vacancy orderings for Na_xCrO_2.

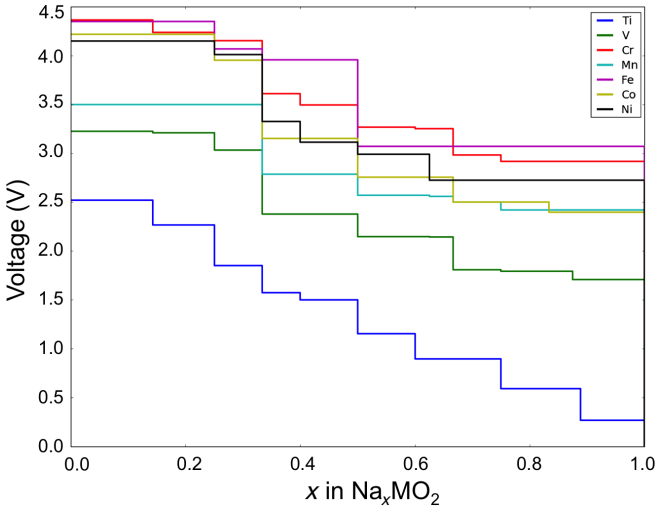

FIG. 5. Computed voltage curves for Na_xMO_2 (M = Ti, V, Cr, Mn, Fe, Co, and Ni). The voltage is referenced against Na metal.

these systems nontopotactic structural changes away from $O3$ may occur.

All single-layer Na-vacancy orderings that appear as a ground state in one or more of the seven systems form the set of 18 structures shown in Fig. 6. Several of the ground-state orderings have a fairly homogeneous distribution of vacancies and Na [e.g., Figs. 6(a)–6(c)], while others show vacancy clustering in regularly distributed lines [e.g., Figs. 6(m), 6(n), and 6(p)]. Figure 6(j) shows a unique ground state found experimentally and confirmed computationally in earlier work [27] in which Na ions are relaxed out of their original octahedral sites into distorted octahedra. This structure does not appear as a ground state in TM oxide systems other than the Ni and Mn systems and is related to the strong Jahn-Teller coupling in these systems.

Some Na-vacancy orderings are present with their symmetrically equivalent structure obtained by exchanging Na ions and vacancies. For example, Figs. 6(b) and 6(o) and Figs. 6(d) and 6(l) represent equivalent orderings. It is remarkable, however, how many of the ground-state Na orderings do not occur with their equivalent vacancy pattern. This can occur only if the effective Hamiltonian describing the Na-vacancy interactions is highly asymmetric around $x = 1/2$ due to the presence of strong effective many-body interactions [36]. Note that electrostatic interactions, often thought to dominate cation-vacancy ordering, would create a more symmetric system, as their ground-state solution is symmetric with respect to Na and vacancies [37]. Hence, the strong asymmetry in the possible ground states in Fig. 6 indicates that effective many-body interactions play an important role. Such many-body interactions can be caused by elastic effects or strong coupling between Na-vacancy ordering and the local electronic structure.

We explore how close to the convex hull each of the candidate orderings in Fig. 6 is for each Na_xMO_2 system. These results are summarized in Fig. 7. The darkest squares

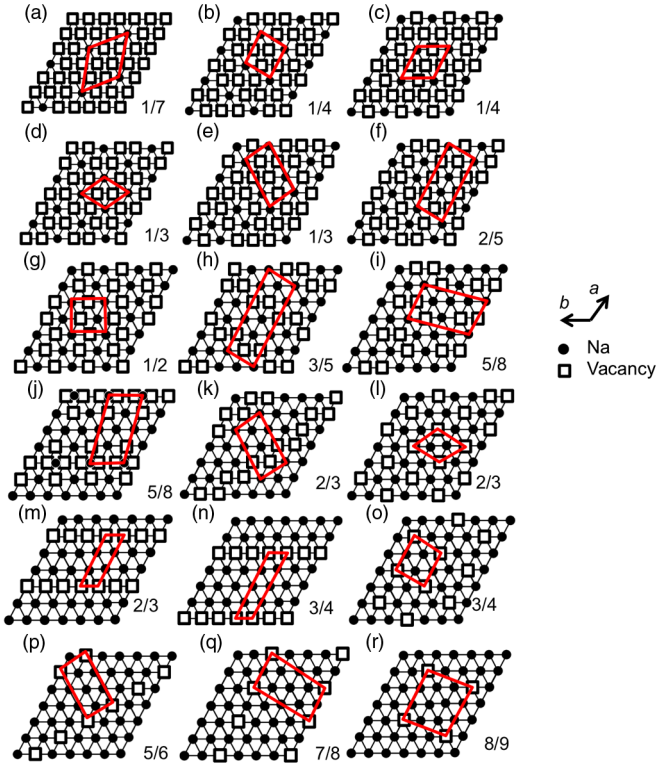

FIG. 6. (a)–(r) Na-vacancy ordering in single-layer phases found as ground-state phases in Na_xMO_2 voltage curves (M = Ti, V, Cr, Mn, Fe, Co, and Ni). (j) depicts a Na ordering described by Li *et al.* [27] where Na ions are relaxed out of their conventional octahedral sites.

indicate that the ordering type as defined in Fig. 6 is a ground state in the particular $O3$ TM oxide system. Lighter squares in the figure indicate that a structure is not a ground state but is within 0–10 and 10–20 meV per atom of the convex hull, respectively. The lightest color indicates the structure is calculated but is more than 20 meV away from the hull. It is clear from the data in Fig. 7 that similar

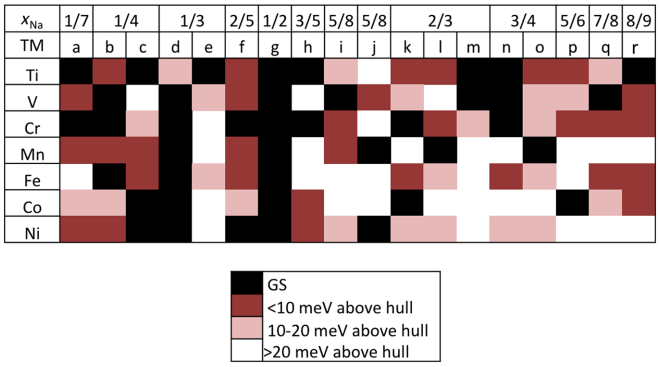

FIG. 7. Energy above the hull for Na_xMO_2 versions of each Na-vacancy ordering type (a)–(r) shown in Fig. 6. The lightest spaces indicate that the structure has been calculated for the transition-metal system in question but does not appear within 20 meV of the hull for that system.

orderings appear as ground-state phases for multiple TM oxide systems. The structure shown in Fig. 6(g) for $x_{Na} = 1/2$ appears as a stable state in all seven TM systems. For $x_{Na} = 1/3$, all seven TM systems have a ground-state phase, and six of these have the same Na ordering, the electrostatically favorable $\sqrt{3} \times \sqrt{3}$ ordering [Fig. 6(d)] [38]. While the remaining Ti system has another ground state for $x_{Na} = 1/3$, the energy of the $\sqrt{3} \times \sqrt{3}$ structure is within 20 meV of the hull.

The Ti and Cr systems have a stable ground state at each composition in Fig. 7, and many of the non-ground-state orderings are close to the convex hull. This indicates a strong degeneracy of ordering energies, which can be caused by either small interactions or long-range frustrated interactions. Some of the competing structures are within 5 meV/f.u. of the ground state, implying that entropy effects at finite temperatures or minor compositional variations (as, for example, those caused by different synthesis techniques) may lead to a different phase. A degeneracy in phases together with a shallow voltage curve and small voltage steps is likely to lead to faster kinetics while cycling through phase transitions and thus would imply a better rate capability in the cathode. The concentration differences between phase transitions correlate to the ease of nucleation of the new phase, and the height of each phase-transition step corresponds to the energy difference between phases. Thus, the Cr and Ti voltage curves indicate better possible kinetics, because they have multiple shallow steps. In the Fe system, ground-state structures are comparatively more stable than competing ordered structures, which are typically more than 10 meV higher in energy, implying that the phases forming in the Fe system are nondegenerate and have higher energetic boundaries (and thus slower kinetics) in cycling. Results similar to Fe can be seen in the Co and Ni systems.

While our results indicate that the total number of distinct ground-state Na-vacancy orderings that can be stable is remarkably small, there is significant variation of the ground-state set among different TM systems. This implies that the TM selection influences the preferred Na-vacancy ordering, either structurally or electronically. Because of the relatively small energy range within which different orderings appear above the hull for each TM system, we investigate to what extent the adjacent Na layer interaction (position of Na ordering relative to that of an adjacent layer, or layer "stacking") can influence the energy of the system and determine the preferred ground state. Such long-range interlayer interactions are known to be related in part to the electronic structure configuration of the TM ion [27,29].

B. Influence of stacking on energy in *O*3-type layered oxides

To investigate the interlayer interaction, we enumerate all distinct lateral translations of the Na pattern in adjacent layers (no rotation of ordering) generated by all linear combinations of primitive vector directions parallel to the Na layer. This leads to between two and six different possible configurations for each pattern. Figure 8 shows the difference in energy between the highest and lowest energy stacking for each Na concentration, transition metal, and ordering type. High total bars (as for orderings "j" and "o," for example) imply that, in general, the 3D stacking of that ordering strongly influences energy regardless of TM, while for orderings such as "m" and "l" stacking has little effect on the energy. The size of each color-coded bar indicates the difference for that TM. For example, stacking clearly has more influence on energy in Na_xCoO_2 (orange bars) than Na_xCrO_2 (green bars). We find that the effect of layer stacking on energy within a single ordering type is small compared to the effect of Na-vacancy ordering; however, it is non-negligible. The energy difference between the highest and lowest energy stacking depends on the Na concentration and transition metal in the system but is generally less than 30 meV per Na_xMO_2 formula unit. The system with ordering type "j" is relatively strongly affected by stacking, because the Na ions in this ordering exist in highly distorted sites due to a correlated effect across layers, so changing their layer stacking increases the energy significantly. It is expected that orderings that have only a small energy change when the stacking changes will have frequent stacking faults and as such may be more difficult to detect in diffraction.

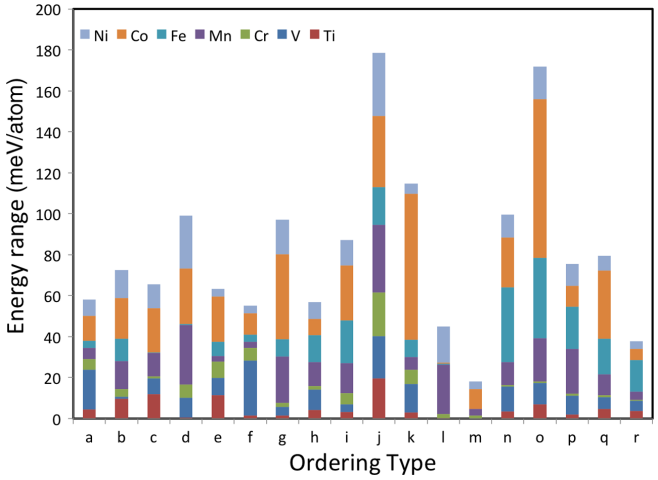

FIG. 8. Energy difference between the highest and lowest energy stacking of the 18 low-energy orderings in seven TM systems. The letters refer to the structures as shown in Fig. 6. The size of each color-coded bar gives the energy difference between the highest and lowest energy stacking for that TM and ordering type. Hence, high total bars as for orderings "j" and "o" indicate that, in general, the 3D stacking of that ordering strongly influences the energy, while for orderings such as "m" and "l" there is very little effect of stacking on the energy.

Desodiation of $NaMO_2$ creates a $3+/4+$ mixed valence on the transition metal. For many TM oxides, the mixed

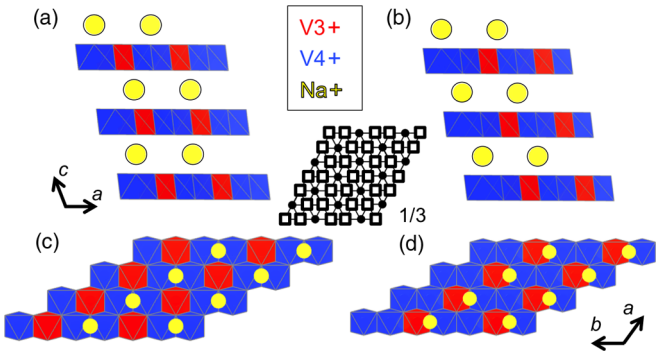

FIG. 9. Comparison of oxidation state ordering between two stacking variations of the $x_{Na} = 1/3$ ordering shown in Fig. 6(d), in the *O*3 host. (a) and (c) show the TM oxidation state ordering across three layers and in a single Na layer, respectively. This ordering is 10 meV higher than that in (b) and (d). Red octahedra indicate V^{3+} ions, while blue octahedra indicate V^{4+} ions. The difference in stacking of adjacent layers can be seen as a glide of the middle Na layer while the top and bottom layers remain stationary.

valence is accommodated by the distribution of discrete M^{3+} and M^{4+} ions. Hence, Na-vacancy ordering can be accompanied by charge ordering on the TM sites. For systems such as *P*2-Na_xCoO_2 [39] and Li_xFePO_4 [40], such coupling is well documented. We perform a preliminary analysis of this coupling in the V system. Figure 9 shows the Na-vacancy ordering and the oxidation state ordering in the TM oxide layer in two stacking variants of a ground state of the V system. Figure 9(c) shows the TM ion oxidation state ordering in each TM oxide layer. The Na-vacancy ordering in this structure is that of Fig. 6(d), with 1/3 Na concentration patterned in a $\sqrt{3} \times \sqrt{3}$ ordering, which allows for two possible stackings of adjacent Na layers. The red octahedra represent V^{3+}, and blue octahedra represent V^{4+}. Figure 9(a) shows the stacking with an energy 10 meV higher than that of Fig. 9(b). Though the TM oxidation state ordering is the same in each of the TM oxide layers, their relative position to the Na layers and to each other changes with stacking.

IV. DISCUSSION

A. Comparison to experiments

The objective of our study is to investigate the common Na-vacancy orderings that can occur in Na_xMO_2 systems. By extensively calculating seven *O*3 Na_xMO_2 systems, 18 unique single-layer ordering types are found, many of which occur repeatedly in several TM systems. Though few Na-vacancy-ordered phases are fully characterized in *O*3-type Na-ion intercalation systems, the experimental results available are in good agreement with our observations. Direct comparison with experiments is possible for systems where transition into a *P*3 host does not occur during cycling, such as Na_xVO_2 [17] and Na_xTiO_2 [41].

The voltage plots in this study are computed at 0 K, and, while temperature can have an effect on whether weakly ordered phases are observed, previous work has shown that 0-K phases are good indicators of the phases present at room temperature. In $LiCoO_2$ and $LiNiO_2$, for example, where finite-temperature phase diagrams have been computed and derived experimentally, low-temperature ground-state phases are apparent to well above 300 K [25,29]. Because of its relative ionic radius, Na-ion ordering is predicted to be stronger than that of Li ions, leading to even higher disordering temperatures, making experimental validation of this study viable. Indeed, ordering is observed experimentally in Na-intercalating layered oxides, which show numerous voltage steps and plateaus indicating ordering phase transitions even at relatively high cycling rates of $C/20$ or $C/10$ [15,16,42,43]. The degeneracy of phases as uncovered in this study can be an indicator of relative disordering temperatures, with highly degenerate systems tending to lower disordering temperatures.

Figure 10 shows a comparison of the calculated voltage curve with the experimentally measured voltage for Na_xVO_2 which cycles in an *O*3-type phase between $NaVO_2$ and $Na_{1/2}VO_2$. The agreement between the measured and calculated voltage curves is quite good in terms of Na concentration and voltage matching at phase transitions (steps and plateaus), with the experimental curve falling within 0.1 V of the computed curve at most points. Phase transition positions match at 2/3, 5/8, and 1/2 Na concentrations, and, in particular, the phase transition at $x_{Na} = 2/3$ matches the computed curve well, with a step height of approximately 0.4 V compared to the computed 0.5 V. The computationally predicted ground states at 3/4 and 7/8 are not apparent in the experimental curve; however, it is possible that these are smoothed away at a finite temperature due to entropic effects. Additionally, the

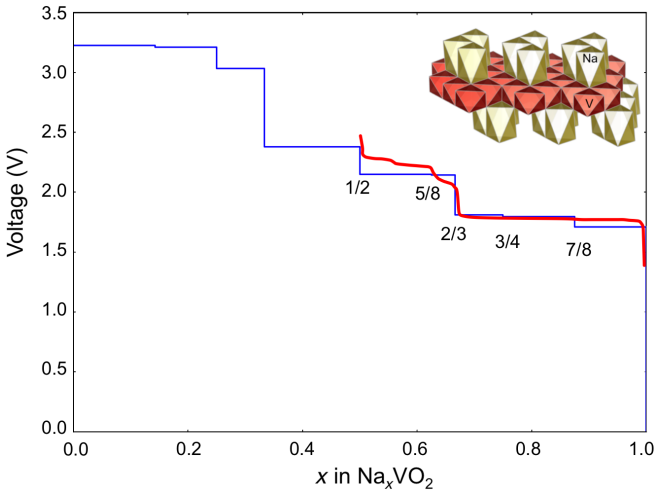

FIG. 10. Computed and experimental voltage curve of *O*3-Na_xVO_2. Inset: Predicted ground state for *O*3-$Na_{1/2}VO_2$ also observed experimentally [17].

ground-state vacancy ordering of $Na_{1/2}VO_2$ predicted by this study as described by Fig. 6(d) matches that characterized by Didier in 2012. The predicted ground-state layer stacking is also correct [17]. The comparison captures some limitations to our methods, however, as the experimental curve shows an additional first-order phase transition between $x_{Na} = 0.5$ and $x_{Na} = 0.6$ which is missing from the computed results.

In several systems (M = Cr, Co, Ni), the fully sodiated phase exists in the $O3$ structural configuration, but the $P3$ phase appears after approximately 0.2–0.4 Na is deintercalated from the stoichiometric $NaMO_2$ phase. In these systems, direct comparison with $O3$-phase calculated voltage plots is possible only in parts of the experimental curves where the $O3$ system is more stable. In several single TM layered oxide systems, an irreversible phase transformation [44] is apparent when the cathode is charged beyond a particular capacity (typically, $x_{Na} = 0.3$–0.5 in Na_xMO_2). This irreversibility is thought to come from transition-metal ion migration into the alkali layer, as has been evidenced in the Fe, Cr, and Ti systems [6,45,46]. Therefore, for low Na concentrations, a direct comparison with experimental results is not possible, but our calculations suggest likely topotactic ground states at lower Na concentrations.

B. Common ground-state phases in $O3$ single TM oxides

Our results give rise to several interesting implications that can be used to predict alkali orderings in layered metal oxide structures. We look closely at the Cr system and results from several other TM oxide systems as examples. We see effects on ground-state phase vacancy homogeneity and degeneracy of phases as well as the influence of the Jahn-Teller effect in our analysis.

Electrostatic interaction is clearly an important influence on ground-state ordering. As electrostatics is a repulsive interaction, one expects it to drive the minority species (Na for $x < 1/2$ or vacancies for $x > 1/2$) as far away from each other as possible leading to a "homogeneous" structure. This is evidenced in our candidate set of orderings, where such "homogeneously distributed" Na-ion patterns are seen as ground states for multiple TM oxide systems, e.g., Figs. 6(a)–6(c). In several of the systems studied, however, the ground-state phases have minority species which are clustered in lines or rows, indicating that pure Na-Na or vacancy-vacancy electrostatic repulsion is not the only contribution to the energy. For example, the Cr system described in Fig. 4 shows vacancies clustered in rows within the alkali layer at $x_{Na} = 3/4$ and $2/3$. Such "less homogeneous" ordering requires some attractive interactions between like species. Attractive interactions are caused either by direct hybridization, unlikely for Na ions, or by elastic interactions mediated through the solid [47]. The presence of these interactions and their associated orderings is consistent with the strain associated by inserting or removing the large Na^+ ion.

The Cr system shows many structures very close in energy and near the hull, implying a number of energetically degenerate phases at each Na concentration. A highly degenerate phase is more likely to disorder at lower temperatures, as only small fluctuations in energy are needed for the system to move between ordered phases. The Cr system can access these phases easily, as indicated by a voltage curve with low slope and voltage steps that are relatively small for $1/2 \leq x_{Na} \leq 1$. The Fe system shows a different trend than Cr: We see nondegenerate Na-vacancy orderings, implying stronger ordered phases. Indeed in Na_xFeO_2, the $x = 1/2$ ground state is so dominant that it creates a two-phase region for $1/2 \leq x_{Na} \leq 1$. One component to the difference between the Cr and Fe systems is their electronic structure. Cr^{3+} and Cr^{4+} ions are present in the partially sodiated phases, neither of which have e_g electrons, while high spin Fe^{3+} and Fe^{4+} have two and one unpaired e_g electrons, respectively. It has been demonstrated that e_g electrons couple to alkali ordering more strongly than t_{2g} states [29], and hence Fe ions have stronger influence on Na-vacancy ordering.

Ni^{3+} and Mn^{3+} ions are strongly Jahn-Teller active, meaning their TM-O bonds are distorted in the octahedral complex. Therefore, the Ni and Mn systems typically exhibit similar Na-vacancy orderings which are different from the other non-Jahn-Teller active TM systems. This is seen in Fig. 7, wherein Ni and Mn systems exhibit the same ground-state Na ordering at $x_{Na} = 1/3$, $1/2$, and $5/8$. The Mn and Ni systems both exhibit an unusual ground state at $5/8$ Na concentration [Fig. 6(j)], where the Na ions are distorted from their regular octahedral sites. This has been confirmed experimentally for the Mn system [27]. This distortion has not been investigated for other Na concentrations.

C. Comparison to Li systems

Only a small number of layered $LiMO_2$ systems have been investigated for Li-vacancy ordering, as only the Co and Ni systems show reversible intercalation among the single transition-metal $LiMO_2$ systems. The $O3$-Li_xCoO_2 system has been studied both experimentally and computationally [24,25,48,49]. Computational studies of the phase diagram reveal that the $O3$ host structure is stable above $x_{Li} = 0.3$, below which the H1–3 host is stable with an ordered structure at $x_{Li} = 1/6$. Computationally, ordered ground states in the $O3$ host are found at $x_{Li} = 1/3$, $2/5$, $1/2$, $3/5$, $2/3$, $3/4$, $5/6$, $6/7$, and $8/9$ [24,25]. The phases at $x_{Li} = 2/3$ and $x_{Li} = 1/3$ exhibit the $\sqrt{3} \times \sqrt{3}$ patterns in Figs. 6(l) and 6(d), respectively (this ordering is also predicted to be present in alternating $O3$ layers in the H1–3 structure at $x_{Li} = 1/6$), and the phase at $x_{Li} = 3/4$ has $c(2 \times 4)$ vacancy ordering as in Fig. 6(o). The $Li_{1/2}CoO_2$ ordering is confirmed experimentally [48,49] and is a 2×1 ordering where the alkali ions form rows on the triangular lattice [24,48,49]. This ordering is investigated

for our study and found to be within 20 meV/f.u. of the hull for all Na systems. Figure 6(g) ordering in this study is conversely found to be a near-degenerate state in Li_xCoO_2, just 1 meV/f.u. away from the convex energy hull [25].

The Li_xNiO_2 voltage curve is shown computationally and experimentally to exhibit ordering phases at room temperature at $x_{Li} = 1/4, 1/3, 2/5, 1/2$, and $3/4$ [23]. The voltage curve differs significantly from that of Li_xCoO_2, as the presence of Jahn-Teller active Ni^{3+} ions in this structure results in interplane interactions between Li ions. Several of the orderings found to be ground states in this system are found in the set of 18 described here. $Li_{1/3}NiO_2$ and $Li_{1/4}NiO_2$ [50] are characterized experimentally and shown to be the same as the Figs. 6(d) and 6(c) patterns predicted in this study. The orderings predicted computationally by Arroyo y de Dompablo in the Li_xNiO_2 system but not described experimentally also match those in the set of 18, for $x_{Li} = 2/5$ [Fig. 6(f)] and $3/4$ [Fig. 6(o)] [23]. These findings indicate that the set of 18 orderings described in this work can also function as potential candidates for non-Na alkali-ordered structures.

V. CONCLUSIONS

Through thorough DFT computation, we predict voltage curves and stable Na-vacancy orderings for seven Na_xMO_2 *O*3 compounds. We find 18 orderings that appear as ground states in one or more of the seven TM systems. Several appear as ground states in more than one system.

While some Na-vacancy orderings are the electrostatically favored pattern, the lack of symmetry of the ground states around $x_{Na} = 1/2$ and the presence of ground states with inhomogeneous Na-vacancy distributions point to other contributions such as ionic relaxation and electronic structure contributions to the effective Na-vacancy interactions. We believe that these 18 ground-state structures form a good set of candidate structures to refine the Na-vacancy ordering in more complex Na_xMO_2 systems.

ACKNOWLEDGMENTS

We thank the Samsung Advanced Institute of Technology for funding of this research and acknowledge computing time at the National Energy Research Scientific Computing Center, a DOE Office of Science User Facility supported by the Office of Science of the U.S. Department of Energy under Contract No. DE-AC02-05CH11231. We acknowledge Rahul Malik, Xin Li, and Xiaohua Ma for helpful discussions.

[1] M. D. Slater, D. Kim, E. Lee, and C. S. Johnson, Sodium ion batteries, Adv. Funct. Mater. **23**, 947 (2013).

[2] S. Komaba, W. Murata, T. Ishikawa, N. Yabuuchi, T. Ozeki, T. Nakayama, A. Ogata, K. Gotoh, and K. Fujiwara, Electrochemical Na insertion and solid electrolyte interphase for hard-carbon electrodes and application to Na-ion batteries, Adv. Funct. Mater. **21**, 3859 (2011).

[3] S. Kim, D. Seo, X. Ma, G. Ceder, and K. Kang, Electrode materials for rechargeable sodium-ion batteries: Potential alternatives to current lithium-ion batteries, Adv. Energy Mater. **2**, 710 (2012).

[4] S. P. Ong, V. L. Chevrier, G. Hautier, A. Jain, C. Moore, S. Kim, X. Ma, and G. Ceder, Voltage, stability and diffusion barrier differences between sodium-ion and lithium-ion intercalation materials, Energy Environ. Sci. **4**, 3680 (2011).

[5] N. Yabuuchi, K. Kubota, M. Dahbi, and S. Komaba, Research development on sodium-ion batteries, Chem. Rev. **114**, 11636 (2014).

[6] A. Maazaz, C. Delmas, and P. Hagenmuller, A study of the Na_xTiO_2 system by electrochemical deintercalation, J. Inclusion Phenom. **1**, 45 (1983).

[7] C. Didier, M. Guignard, C. Denage, O. Szajwaj, S. Ito, I. Saadoune, J. Darriet, and C. Delmas, Electrochemical Na-deintercalation from $NaVO_2$, Electrochem. Solid State Lett. **14**, A75 (2011).

[8] J. J. Braconnier, C. Delmas, and P. Hagenmuller, Etude par desintercalation electrochimique des systemes Na_xCrO_2 et Na_xNiO_2, Mater. Res. Bull. **17**, 993 (1982).

[9] S. Komaba, C. Takei, T. Nakayama, A. Ogata, and N. Yabuuchi, Electrochemical intercalation activity of layered $NaCrO_2$ vs. $LiCrO_2$, Electrochem. Comm. **12**, 355 (2010).

[10] A. Mendiboure, C. Delmas, and P. Hagenmuller, Electrochemical intercalation and deintercalation of Na_xMnO_2 bronzes, J. Solid State Chem. **57**, 323 (1985).

[11] Y. Takeda, K. Nakahara, M. Nishijima, N. Imanishi, and O. Yamamoto, Sodium deintercalation from sodium iron oxide, Mater. Res. Bull. **29**, 659 (1994).

[12] C. Delmas, J. Braconnier, C. Fouassier, and P. Hagenmuller, Electrochemical intercalation of sodium in Na_xCoO_2 bronzes, Solid State Ionics **3–4**, 165 (1981).

[13] S. Kikkawa, S. Miyazaki, and M. Koizumi, Electrochemical aspects of the deintercalation of layered AMO_2 compounds, J. Power Sources **14**, 231 (1985).

[14] X. Li, D. Wu, Y. Zhou, L. Liu, X. Yang, and G. Ceder, *O*3-type $Na(Mn_{0.25}Fe_{0.25}Co_{0.25}Ni_{0.25})O_2$: A quaternary layered cathode compound for rechargeable Na ion batteries, Electrochem. Comm. **49**, 51 (2014).

[15] X. Ma, H. Chen, and G. Ceder, Electrochemical properties of monoclinic $NaMnO_2$, J. Electrochem. Soc. **158**, A1307 (2011).

[16] P. Vassilaras, X. Ma, X. Li, and G. Ceder, Electrochemical properties of monoclinic $NaNiO_2$, J. Electrochem. Soc. **160**, A207 (2013).

[17] C. Didier, M. Guignard, J. Darriet, and C. Delmas, O'3-Na_xVO_2 system: A superstructure for $Na_{1/2}VO_2$, Inorg. Chem. **51**, 11007 (2012).

[18] M. Guignard, C. Didier, J. Darriet, P. Bordet, E. Elkaim, and C. Delmas, P2-Na_xVO_2 system as electrodes for batteries and electron-correlated materials, Nat. Mater. **12**, 74 (2012).

[19] C. Delmas, C. Fouassier, and P. Hagenmuller, Structural classification and properties of the layered oxides, Physica (Amsterdam) **99B**, 81 (1980).

[20] Z. Lu and J. R. Dahn, In situ x-ray diffraction study of P2-$Na_{2/3}[Ni_{1/3}Mn_{2/3}]O_2$, J. Electrochem. Soc. **148**, A1225 (2001).

[21] Y. S. Meng, Y. Hinuma, and G. Ceder, An investigation of the sodium patterning in Na_xCoO_2 (0.5×1.0) by density functional theory methods, J. Chem. Phys. **128**, 104708 (2008).

[22] Y. Wang, Y. Ding, and J. Ni, Ground-state phase diagram of Na_xCoO_2: Correlation of Na ordering with CoO_2 stacking sequences, J. Phys. Condens. Matter **21**, 035401 (2009).

[23] M. E. Arroyo y de Dompablo, A. Van der Ven, and G. Ceder, First-principles calculations of lithium ordering and phase stability on Li_xNiO_2, Phys. Rev. B **66**, 064112 (2002).

[24] C. Wolverton and A. Zunger, First-Principles Prediction of Vacancy Order-Disorder and Intercalation Battery Voltages in Li_xCoO_2, Phys. Rev. Lett. **81**, 606 (1998).

[25] A. Van der Ven, M. K. Aydinol, G. Ceder, G. Kresse, and J. Hafner, First-principles investigation of phase stability in Li_xCoO_2, Phys. Rev. B **58**, 2975 (1998).

[26] Y. Wang, R. Xiao, Y. Hu, M. Avdeev, and L. Chen, P2-$Na_{0.6}[Cr_{0.6}Ti_{0.4}]O_2$ cation-disordered electrode for high-rate symmetric rechargeable sodium-ion batteries, Nat. Commun. **6**, 6954 (2015).

[27] X. Li, X. Ma, D. Su, L. Liu, R. Chisnell, S. P. Ong, H. Chen, A. Toumar, J. Idrobo, Y. Lei, J. Bai, F. Wang, J. W. Lynn, Y. S. Lee, and G. Ceder, Direct visualization of the Jahn-Teller effect coupled to Na ordering in $Na_{5/8}MnO_2$, Nat. Mater. **13**, 586 (2014).

[28] M. Kaburagi and J. Kanamori, Ground state structure of triangular lattice gas model with up to 3rd neighbor interactions, J. Phys. Soc. Jpn. **44**, 718 (1978).

[29] M. E. Arroyo y de Dompablo and G. Ceder, First-principles calculations on Li_xNiO_2: Phase stability and monoclinic distortion, J. Power Sources **119–121**, 654 (2003).

[30] A. Jain, G. Hautier, C. J. Moore, S. P. Ong, C. C. Fischer, T. Mueller, K. A. Persson, and G. Ceder, A high-throughput infrastructure for density functional theory calculations, Comput. Mater. Sci. **50**, 2295 (2011).

[31] G. Kresse and J. Furthmueller, Effective iterative schemes for *ab initio* total-energy calculations using a plane-wave basis set, Phys. Rev. B **54**, 11169 (1996).

[32] P. E. Bloechl, Projector augmented-wave method, Phys. Rev. B **50**, 17953 (1994).

[33] J. P. Perdew, M. Ernzerhof, and K. Burke, Rationale for mixing exact exchange with density functional approximations, J. Chem. Phys. **105**, 9982 (1996).

[34] V. I. Anisimov, F. Aryasetiawan, and A. I. Lichtenstein, First-principles calculations of the electronic structure and spectra of strongly correlated systems: The LDA + U method, J. Phys. Condens. Matter **9**, 767 (1997).

[35] M. K. Aydinol, A. F. Kohan, G. Ceder, K. Cho, and J. Joannopoulos, *Ab initio* study of lithium intercalation in metal oxides and metal dichalcogenides, Phys. Rev. B **56**, 1354 (1997).

[36] G. Ceder, H. Dreyssé, and D. de Fontaine, Triplet interactions and the $C(2 \times 2)$ overlayer phase diagram, Physica (Amsterdam) **193A**, 105 (1993).

[37] G. Ceder and A. Van der Ven, Phase diagrams of lithium transition metal oxides: First-principles investigations, Electrochim. Acta **45**, 131 (1999).

[38] Y. Saito and G. Tabe, $\sqrt{3} \times \sqrt{3}$ structure on the triangular lattice, J. Phys. Soc. Jpn. **54**, 2955 (1985).

[39] Y. Hinuma, Y. S. Meng, and G. Ceder, Temperature-concentration phase diagram of P2-NaxCoO2 from first-principles calculations, Phys. Rev. B **77**, 224111 (2008).

[40] F. Zhou, T. Maxisch, and G. Ceder, Configurational Electronic Entropy and the Phase Diagram of Mixed-Valence Oxides: The Case of Li_xFePO_4, Phys. Rev. Lett. **97**, 155704 (2006).

[41] D. Wu, X. Li, B. Xu, N. Twu, L. Liu, and G. Ceder, $NaTiO_2$: A layered anode material for sodium-ion batteries, Energy Environ. Sci. **8**, 195 (2015).

[42] D. Hamani, M. Ati, J.-M. Tarascon, and P. Rozier, Na_xVO_2 as possible electrode for Na-ion batteries, Electrochem. Comm. **13**, 938 (2011).

[43] M. H. Han, E. Gonzalo, M. Casas-Cabanas, and T. Rojo, Structural evolution and electrochemistry of monoclinic $NaNiO_2$ upon the first cycling process, J. Power Sources **258**, 266 (2014).

[44] S. Komaba, T. Nakayama, A. Ogata, T. Shimizu, C. Takei, S. Takada, A. Hokura, and I. Nakai, Electrochemically reversible sodium intercalation of layered $NaNi_{0.5}Mn_{0.5}O_2$ and $NaCrO_2$, ECS Trans. **16**, 43 (2009).

[45] N. Yabuuchi, H. Yoshida, and S. Komaba, Crystal structures and electrode performance of alpha-$NaFeO_2$ for rechargeable sodium batteries, Electrochemistry **80**, 716 (2012).

[46] K. Kubota, I. Ikeuchi, T. Nakayama, C. Takei, N. Yabuuchi, H. Shiiba, M. Nakayama, and S. Komaba, New insight into structural evolution in layered $NaCrO_2$ during electrochemical sodium extraction, J. Phys. Chem. C **119**, 166 (2015).

[47] G. Ceder, P. D. Tepesch, A. F. Kohan, and A. Van der Ven, A model to predict ionic disorder and phase diagrams: Application to CaO-MgO, Gd_2O_3-ZrO_2 and to sodium β"-alumina', J. Electroceram. **1**, 15 (1997).

[48] J. N. Reimers and J. R. Dahn, Electrochemical and *in situ* x-ray diffraction studies of lithium intercalation in Li_xCoO_2, J. Electrochem. Soc. **139**, 2091 (1992).

[49] Y. Shao-Horn, S. Levasseur, F. Weill, and C. Delmas, Probing lithium and vacancy ordering in *O*3 layered Li_xCoO_2 ($x \approx 0.5$), J. Electrochem. Soc. **150**, A366 (2003).

[50] C. Chazel, M. Menetrier, L. Croguennec, and C. Delmas, Coupled ion/electron hopping in Li_xNiO_2: A ^{7}Li NMR study, Inorg. Chem. **45**, 1184 (2006).